





# Machine Learning Radiomics Model for External and Internal Respiratory Motion Correlation Prediction in Lung Tumor

Technology in Cancer Research & Treatment  
Volume 21: 1-11  
© The Author(s) 2022  
Article reuse guidelines:  
sagepub.com/journals-permissions  
DOI: 10.1177/15330338221143224  
journals.sagepub.com/home/tct  


Xiangyu Zhang, MM<sup>1</sup>, Xinyu Song, MM<sup>1,2</sup>, Guangjun Li, MS<sup>1</sup> ,  
Lian Duan, BE<sup>3</sup>, Guangyu Wang, MM<sup>1</sup>, Guyu Dai, MM<sup>1</sup>,  
Ying Song, PhD<sup>1</sup>, Jing Li, PhD<sup>1</sup> , and Sen Bai, MS<sup>1,4</sup> 

## Abstract

**Objectives:** The complexity and specificity of lung tumor motion render it necessary to determine the external and internal correlation individually before applying indirect tumor tracking. However, the correlation cannot be determined from patient respiratory and tumor clinical characteristics before treatment. The purpose of this study is to present a machine learning model for an external/internal correlation prediction that is based on computed tomography (CT) radiomic features. **Methods:** 4-dimensional computed tomography (4DCT) images of 67 patients were collected retrospectively, and the external/internal correlation of lung tumor was calculated based on Spearman's rank correlation coefficient. Radiomic features were extracted from average intensity projection and the light gradient boosting machine (LightGBM)-based cross-validation (the recursive elimination method) was used for feature selection. The LightGBM framework forecasting models with classification thresholds 0.7, 0.8, and 0.9 are established using stratified 5-fold cross-validation. Model performance was assessed using receiver operating characteristics, sensitivity, and specificity. **Results:** There were 16, 18, and 13 features selected for models 0.7, 0.8, and 0.9, respectively. Texture features are of great importance in external/internal correlation prediction compared to other features in all models. The sensitivities of the predictions in models 0.7, 0.8, and 0.9 were  $0.800 \pm 0.126$ ,  $0.829 \pm 0.140$ , and  $0.864 \pm 0.086$ , respectively. The specificities were  $0.771 \pm 0.114$ ,  $0.936 \pm 0.0581$ , and  $0.839 \pm 0.101$ , whereas the area under the curve (AUC) was 0.837, 0.946, and 0.877, respectively. **Conclusions:** Our findings indicate that radiomics is an effective tool for respiratory motion correlation prediction, which can extract tumor motion characteristics. We proposed a machine learning framework for correlation prediction in the motion management strategy for lung tumor patients.

## Keywords

lung tumor, respiratory motion, correlation, radiomics, machine learning

Received: August 6, 2022; Revised: August 30, 2022; Accepted: November 17, 2022.

## Introduction

A lung tumor can deform and move significantly owing to respiratory motion,<sup>1,2</sup> which can be up to 3 cm in the superior-inferior (SI) direction, resulting in a huge impact on a radiotherapy outcome.<sup>3</sup> Even if an isotropic 5 mm margin from a clinical target volume (CTV) was generated for respiratory motion compensation, planning target volume (PTV) D95 deviations up to 26% for fractional doses and 14% for total doses in lung stereotactic body radiotherapy were observed.<sup>4</sup> Accurate respiratory motion management can better protect organs at risk (OAR) while maintaining PTV coverage and adequate dose delivery.<sup>5</sup> To better manage the respiratory motion of the tumor, the location of the tumor should be tracked with high spatial and temporal accuracy.<sup>6</sup>

<sup>1</sup> Radiotherapy Physics and Technology Center, Cancer Center, West China Hospital, Sichuan University, Chengdu, China

<sup>2</sup> Department of Radiation Oncology, Cancer Center, The First Affiliated Hospital, Sun Yat-sen University, Guangzhou, China

<sup>3</sup> Department of Radiation Oncology, Perelman School of Medicine, University of Pennsylvania, Philadelphia, PA, USA

<sup>4</sup> Department of Radiation Oncology, Cancer Center, West China Hospital, Sichuan University, Chengdu, China

\*Xiangyu Zhang and Xinyu Song contributed equally to this work.

### Corresponding Authors:

Sen Bai, MS, Radiotherapy Physics and Technology Center, Cancer Center, West China Hospital, Sichuan University, Chengdu, China.  
Email: baisen@scu.edu.cn

Guangjun Li, MS, Radiotherapy Physics and Technology Center, Cancer Center, West China Hospital, Sichuan University, Chengdu, China.  
Email: gjnick829@sina.com



Extensive motion tracking approaches have been proposed and successfully implemented in clinics.<sup>7–11</sup> However, there are limitations with respect to the generality of direct tumor tracking techniques, for example, invasiveness of percutaneous implantation, the risk of pneumothorax or bleeding,<sup>12</sup> clinically acceptable radiation dose for imaging,<sup>13</sup> and migration of the marker.<sup>14</sup> A more clinical and practical tracking approach is to correlate the internal motions with external motions detected by external respiratory surrogates.<sup>10,13,15,16</sup> This is because the external/internal correlation has been evaluated in both linear correlation algorithms and complex models such as support vector regression<sup>17,18</sup> and principal component analysis.<sup>19</sup>

However, respiratory motion and the motion characteristics of a lung tumor vary with each individual.<sup>20,21</sup> The external/internal correlation between external and internal respiratory motion has nothing to do with tumor clinical characteristics such as tumor location, pulmonary function, and size, as well as patient breathing pattern, and other information.<sup>20,22</sup> Other findings suggest that external respiratory motion waveforms do not always accurately correspond to the tumor motion in lung cancer patients,<sup>23</sup> and an external surrogate may not be sufficient to predict complex tumor motion.<sup>24,25</sup> This may lead to the target location being missing when an external surrogate is used to guide treatment in lung cancer patients. Consequently, an individual technology of respiratory motion management is recommended.

In this case, we should not ignore individual differences between patients and use a streamlined tumor movement management plan without additional clinical workload. It is necessary to clarify the tumor motion of a specific patient to determine whether motion management is required and further management methods. The objective of our study is to find an accurate and efficient method to determine the external/internal correlation for specific patients. The correlation can be assessed based on phase shift<sup>26</sup> and the normalization of real-time position management trace data for direct comparison

with the fiducial location.<sup>27</sup> In our previous study, the correlation was calculated considering the Spearman correlation coefficient (SCC) and SCC after support vector regression fitting.<sup>22</sup> However, these methods all require significant additional data acquisition and processing. In the study, we report a novel approach to predict the correlation based on CT radiomic features through machine learning. Radiomics is a means to quantify the radiographic phenotype of a solid tumor via the high-throughput extraction and mining of quantitative features from images acquired from modalities such as CT and magnetic resonance imaging (MRI).<sup>28</sup> The information contained in these features is multidimensional and can be used for precision diagnosis,<sup>29</sup> radiation damage assessment, and prognosis analysis.<sup>30,31</sup> In addition, there have been studies pertaining to respiratory motion on imaging via radiomics and the robustness of radiomic features.<sup>32–34</sup> In this study, we further examined the potential of CT radiomic features in predicting external/internal correlations.

## Materials and Methods

### Patients and Treatment

The study was approved by the ethics committee of West China Hospital with no need for patient consent (No. 2021-86) and registered with the Chinese Clinical trial Registration Center with the registration number “ChiCTR2100042714.” The basic characteristics of 67 patients with lung tumors treated at West China Hospital, between July 2020 and June 2021, were collected (Table 1) to perform a retrospective analysis, with all patient data being anonymized. Patients were treated with image-guided radiation therapy with 54–60 Gy in 2-Gy fractions over 5.5–7 weeks. This study conformed to TRIPOD statements.<sup>35</sup>

All patients underwent a full 4DCT scan in the treatment position under free breathing, which was performed using a Revolution CT instrument (GE Healthcare, Milwaukee, WI, USA). The Varian real-time position management system (Varian Medical Systems, Palo Alto, CA, USA) was used to obtain patient external motion coordinate data. The multiple sets of external real-time motion coordinate data were grouped according to the corresponding respiratory phase, and the average value was used as the external motion data of the phase. Afterward a 4DCT reconstruction with a slice thickness of 3 mm for region of interest (ROI) contouring and treatment planning was performed.

### ROI Segmentation and Evaluation of External/Internal Correlation

A radiation oncologist contoured the gross target volume (GTV) of 10 respiratory phases on a 4DCT based on the Raystation treatment planning system V4.7.6 (RaySearch Laboratories AB, Stockholm, Sweden). Internal tumor motion data are acquired from 4DCT. After CTV contouring, the coordinates of the tumor centroid (Px, Py, and Pz) corresponding to

**Table 1.** Basic Characteristics of the 67 Lung Cancer Patients.

	Lung cancer (67, 95 lesions)	
Motion magnitude of internal tumor $A_i$ (cm)	S-I	$0.887 \pm 0.766$
	A-P	$0.294 \pm 0.299$
	R-L	$0.204 \pm 0.278$
Motion magnitude of the external marker $A_e$ (cm)	$0.957 \pm 0.301$	
Tumor volume $V_t$ (cm <sup>3</sup> )	$14.3 \pm 28.1$	
Patient's age (years)	$58.1 \pm 13.2$	
Gender	Male:female = 46:21	
Lesions	Primary:metastases = 51:44	
Tumor location: lung-wise	Left:right = 38:57	
Tumor location: lobe-wise	Upper:middle:lower = 47:17:31	
Tumor-chest wall	Contact:uncontact = 22:73	
Target lung volume (cm <sup>3</sup> )	573.14–3558.81	

10 respiratory phases were obtained, which were used as internal tumor motion magnitude. According to ESTRO ACROP consensus guideline,<sup>36</sup> employ 0 mm GTV-to-CTV margins. The CTVs are fused on the average intensity projection (AIP) CT to generate 1 internal target volume (ITV). The results were reviewed, edited, and approved by the responsible radiation oncologist, according to our clinical routine. The ITV is the ROI for feature extraction (Figure 1(a)). For patients with multiple tumors, we obtained the internal motion data for each tumor. In this way, we obtained 95 lung ROIs.

The external/ internal correlation was calculated using SCC, which is a nonparametric technique for evaluating the degree of linear association or correlation between 2 independent variables.<sup>37</sup> An SCC value equal to 1 indicates a perfect correlation. The correlation values calculated varied from 0.007 to 0.988, indicating the variability between individual patients. This study mainly focused on the tumor motion in the SI direction because the largest lung tumor motion has been observed in the SI direction (ranging from 3 to 46 mm).<sup>38</sup>

### Feature Extraction

A set of 1218 radiomic features were extracted from ROIs using pyradiomics v3.0.1, which is Imaging Biomarker Standardization Initiative (IBSI)-compliant.<sup>39</sup> The feature definitions described by IBSI are available in a separate document by Zwanenburg et al.<sup>39</sup> All the CTs voxels were resampled to  $1 \times 1 \times 1 \text{ mm}^3$ , the bin width was set to 25 Hounsfield units to increase pattern sensitivity, reducing image noise, and normalizing the intensities. The extracted features include 4 categories (Figure 1(b)): shape features that describe the 3-dimensional (3D) physical appearance of the tumor; first-order features that describe the distribution of the ROI intensities ignoring spatial relations; texture features that describe the interrelationships among voxel intensities using 4 different methods (including gray-level co-occurrence matrix (GLCM), gray-level run length matrix (GLRLM), gray-level size zone matrix (GLSZM), and gray-level dependence matrix (GLDM)); the transform-based features that include the Laplacian of Gaussian and wavelet transforms. We also extracted clinical features, including the volumes of ITV and target lung and the tumor positions based on lung and lobe-wise locations; subsequently, feature engineering was performed.

### Feature Engineering

In this study, light gradient boosting machine-based recursive feature elimination (LightGBM-RFE) was used to select features. The RFE is a feature selection method that fits a model and removes the weakest feature (or features) according to a designated feature ranking standard. Recursion is necessary because for certain measures the relevance of the feature may change substantially when the step-wise elimination process is carried out under a different subset of features. The LightGBM-based RFE algorithm can be expressed as follows:

The training set was denoted by  $X_0 = [X_1, X_2, X_3, \dots, X_N]^T$ , wherein  $X_i$  contains a set of  $m$  features  $F = [f_1, f_2, f_3, \dots, f_m]$  and  $N$  is the size of training set. The class labels were denoted by  $Y = [y_1, y_2, y_3, \dots, y_N]^T$ ,  $y_i \in \{-1, 1\}$  and  $i \in \{1, 2, \dots, N\}$ .

- Step 1: Train a LightGBM model on the initial features set and rank the features by minimizing the mean absolute error.
- Step 2: Determine the feature with smallest ranking criterion and eliminate it.
- Step 3: Update the feature rank.
- Step 4: Repeat Steps 1–3 until the feature  $F$  is empty or the desired number of features remained.

As deciding the number of features should be retained from the feature rank of LightGBM-RFE can have a critical impact, the linear LightGBM-RFE with a stratified-5-fold cross-validation strategy (LightGBM-RFECV) was used to find the minimum feature rank on which the LightGBM model can achieve best performance. The flowchart of the feature selection using LightGBM-RFECV is shown in Figure 1(c).

The feature importance was evaluated based on the  $R^2$  score, which represents the proportion of the variance for a dependent variable that is explained by an independent variable or variables in the model.  $R^2$  score was calculated using the following formula:

$$R^2 = 1 - \frac{\sum_{i=1}^n (z_i - \hat{z}_i)^2}{\sum_{i=1}^n (z_i - \bar{z})^2}$$

where  $z_i$  is the actual value,  $\bar{z}$  is the average value of  $z_i$ , and  $\hat{z}_i$  is the predicted value. A feature with a larger  $R^2$  score is more discriminative.

### Radiomics-Based Predictive Model Building

Based on the radiomic datasets, the classification models were developed using LightGBM. The LightGBM embedded feature dimensionality reduction technology used weak classifiers for training, having high speed and accuracy. Models 0.7, 0.8, and 0.9 were built with classification thresholds with SCC values of 0.7, 0.8, and 0.9, respectively. Kernel Shapley Additive exPlanations (SHAP) were used in 3 models to assess the impact of radiomic features on correlation prediction outcomes. SHAP assigns each feature an importance value for a particular prediction, which is calculated separately without considering any general information regarding the entire model. Kernel SHAP requires fewer evaluations of the original model to obtain similar approximation accuracy.<sup>40</sup> Features with high absolute SHAP values have high importance, whereas low values indicate low importance.

Due to the small sample size, most of the radiomic studies did not use a validation dataset.<sup>41</sup> To improve the stability of the model, the test set was split by stratified sampling to ensure that the test set does not participate in the training of

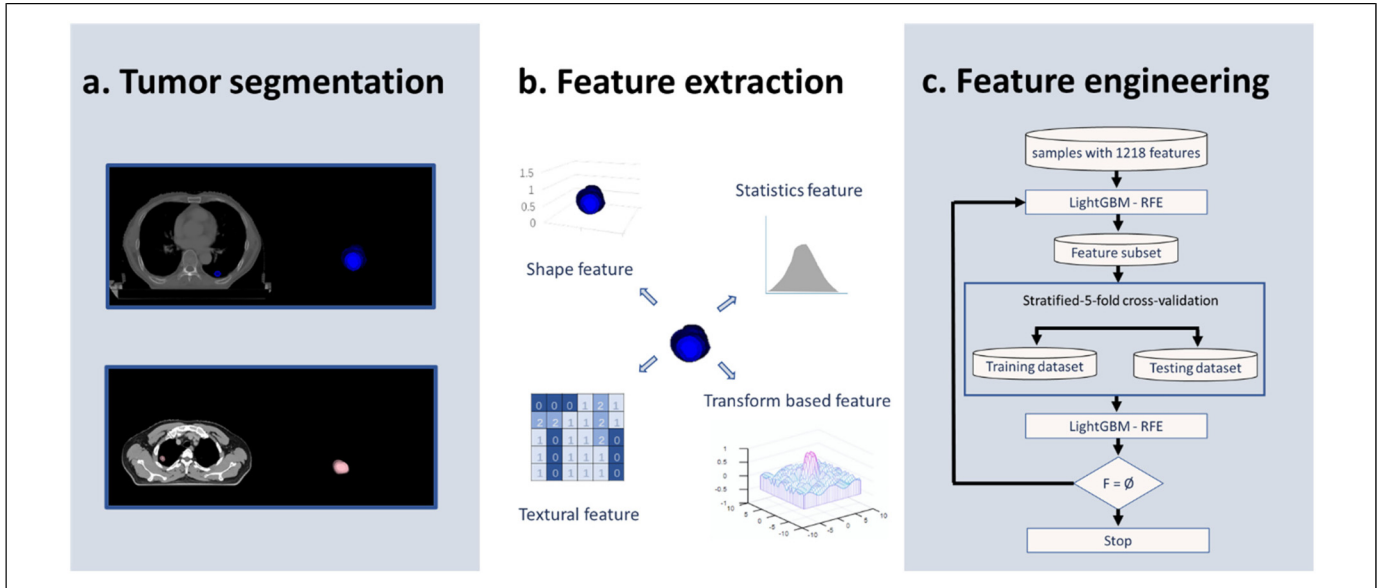


**Figure 1.** Schematic representation of the radiomics workflow. (a) After image preprocessing, the ROI segmentation was performed. (b) Radiomic features including shape features, statistics features, textural features, and transform-based features were extracted. (c) Flowchart of feature engineering based on LightGBM-RFECV.

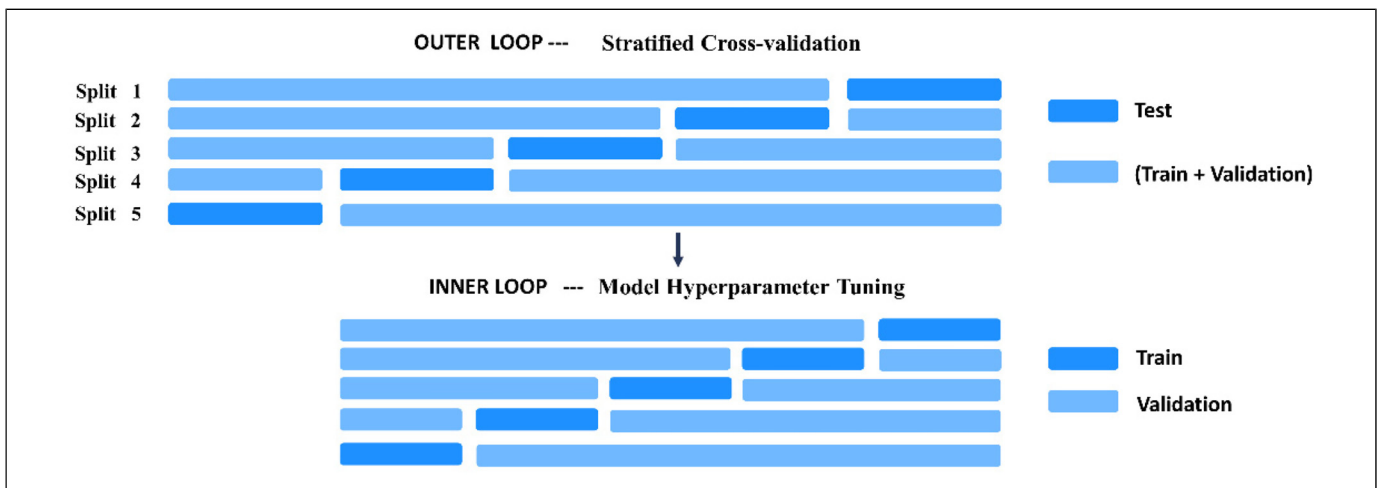


**Figure 2.** Illustration of the structure for a stratified 5-fold cross-validation method.

the model (the same class ratio is preserved throughout all folds). The remaining data were partitioned into 5 equally sized folds. Five iterations of training, validation, and testing were performed subsequently wherein each of the subsamples acted as a validation set (once) and as a part of the training set (4 times). The above training process was performed 5 times to obtain stable results. To avoid the impact of class imbalance on the performance of the model, under- and over-sampling are used to render the number of positive and negative samples as close as possible. This can be achieved by sampling a small number of samples from the majority class and multiple times from a minority class, respectively.<sup>42</sup> A hyperparameter selection process was used to decide the best set of hyperparameters achieving the highest balanced accuracy and perform an

evaluation of model performance. Figure 2 shows the schematic diagram of the training method.

### Statistical Analyses

Model classification forecasting performances were evaluated using: receiver operating characteristic (ROC) curves, AUC, positive predictive values, negative predictive values, sensitivities, specificities, balanced accuracies, and  $F$ -score values. According to the predicted external/internal correlation values, the samples can be classified into 4 types: (1) true positive (TP): both the SCC and predicted value were classified as 1; (2) true negative (TN): both the SCC and predicted value were classified as 0; (3) false positive (FP): the SCC value

was classified as 0 while the predicted value was classified as 1; (4) false negative (FN): the SCC value was classified as 1 while the predicted value was classified as 0. The sensitivities and specificities were calculated as follows:

$$\text{Sensitivity} = \frac{\text{TPs}}{\text{TPs} + \text{FNs}}, \quad (1)$$

$$\text{Specificity} = \frac{\text{TNs}}{\text{TNs} + \text{FPs}}, \quad (2)$$

where an AUC below 0.8 indicated an unsatisfactory accuracy, 0.8 to 0.89 indicated good accuracy, and an AUC greater than 0.9 indicated excellent accuracy.<sup>43</sup>

## Results

### Feature Selection

The selected features with top averaged  $R^2$  scores after feature engineering in each model are shown in Figure 3. For model 0.7, 16 features out of 1218 features were selected. 18 features were selected in model 0.8 while for model 0.9, 13 features were selected. There were 12 common features in the 3 models. Texture features were selected most frequently, including the GLCM, GLSZM, and the GLDM feature while only a few first-order and shape features contributed to the model. No clinical feature was selected.

During the 5 rounds of independent tests, certain features consistently showed high predictive potential for the correlation coefficient between the internal tumor and the external surrogate (CCIE) in each model, and they are as follows: the GLSZM-Gray-level nonuniformity and the GLDM-Large dependence low gray-level emphasis for model 0.7; the first-order maximum and the GLDM-Low gray-level emphasis for model 0.8; the GLDM-Small dependence emphasis and the GLRLM-Long run high gray-level emphasis for model 0.9.

The results evaluating the influence of radiomic features on the CCIE prediction using Kernel SHAP in the 3 models are shown in Figure 4. Colored plots represent SHAP values, and blue and red plots represent lower and higher values, respectively. The SHAP value ranking of features is slightly different from the importance ranking. In the plots of the first-order maximum from model 0.8, the color distribution is opposite to the SHAP value distribution, indicating that the prediction CCIE tends to be negative with a higher maximum. On the contrary, for the GLDM-SDE from model 0.9, red points are distributed in the range of the positive SHAP values, indicating that the CCIE is more likely to be predicted as positive with higher GLDM-SDE.

### Performance of the Radiomics Models

The difference in the performance of the models is summarized in Table 2. When the threshold was 0.7, owing to uneven sample distribution, more than 80% of the samples were negative samples. To improve the performance of the model,

undersampling and oversampling methods were used to balance the positive and negative samples. The sensitivity of the final model was 0.800 and the specificity was 0.771. It can be seen from the obtained results that compared to 0.7, when the threshold was set to 0.8, the sensitivity and specificity of the model improved, with the sensitivity and the specificity being 0.829 and 0.936, respectively. The sensitivity of the model continued to increase (0.864 for model 0.9) as the threshold increased, while the specificity showed a downward trend to 0.839.

The 5-fold combined ROC curves for the 3 models are shown in Figure 5. Model 0.7 demonstrated a performance with an AUC of 0.837, and model 0.8 achieved the best performance with an AUC of 0.946. Model with a threshold of 0.9 achieved an average performance with an AUC of 0.887. The model performance in each fold is provided in Supplementary File 1.

## Discussion

In this study, we emphasized the necessity to determine the external/internal correlation for specific patients and propose a new process to predict the correlation individually via radiomic features specific to a patient. According to our clinical routine, all lung tumor patients accept a 4DCT scan under free breathing for treatment planning, which helps to obtain the motion range of the tumor during respiration. Therefore, the AIP CT generated by a 4DCT contains tumor motion edges within one respiratory cycle and presents this information in imaging with the intensity-spatial distribution of the ROI.

There were 31 radiomic features selected in total, including one shape feature (shape-Maximum 2D diameter column), 4 first-order features, and 24 texture features. First-order features show the ROI voxel intensities distribution based on first-order histograms. Texture features consider the local intensity-spatial distribution in the ROI and provide statistical interrelationships between voxels, which compensate for the loss of information related to the first-order features. Moreover, it has been proven that the texture features extracted by radiomics are not affected by tumor position, size, orientation, and brightness.<sup>44</sup> The features selected for developing the model were highly consistent with those inferred to be sensitive to respiratory motion. Thus, tumor motion information was demonstrated to be obtainable by radiomics.<sup>26</sup>

The radiomic pipelines, including image acquisition, feature extraction, and statistical analyses, vary widely across different studies<sup>27</sup>; therefore, the radiomic features must be focused upon.<sup>45</sup> A radiomic features stability study found that a 4DCT dataset can be used as an alternative to eliminate most of the unstable features as the first step in a feature selection procedure.<sup>46</sup> All features used in our work have a concordance correlation coefficient value above 0.85, signifying a high repeatability and robustness according to their results.

A feature engineering procedure reduces the complexity of the model.<sup>47</sup> It improves the interpretability of the model as well as the

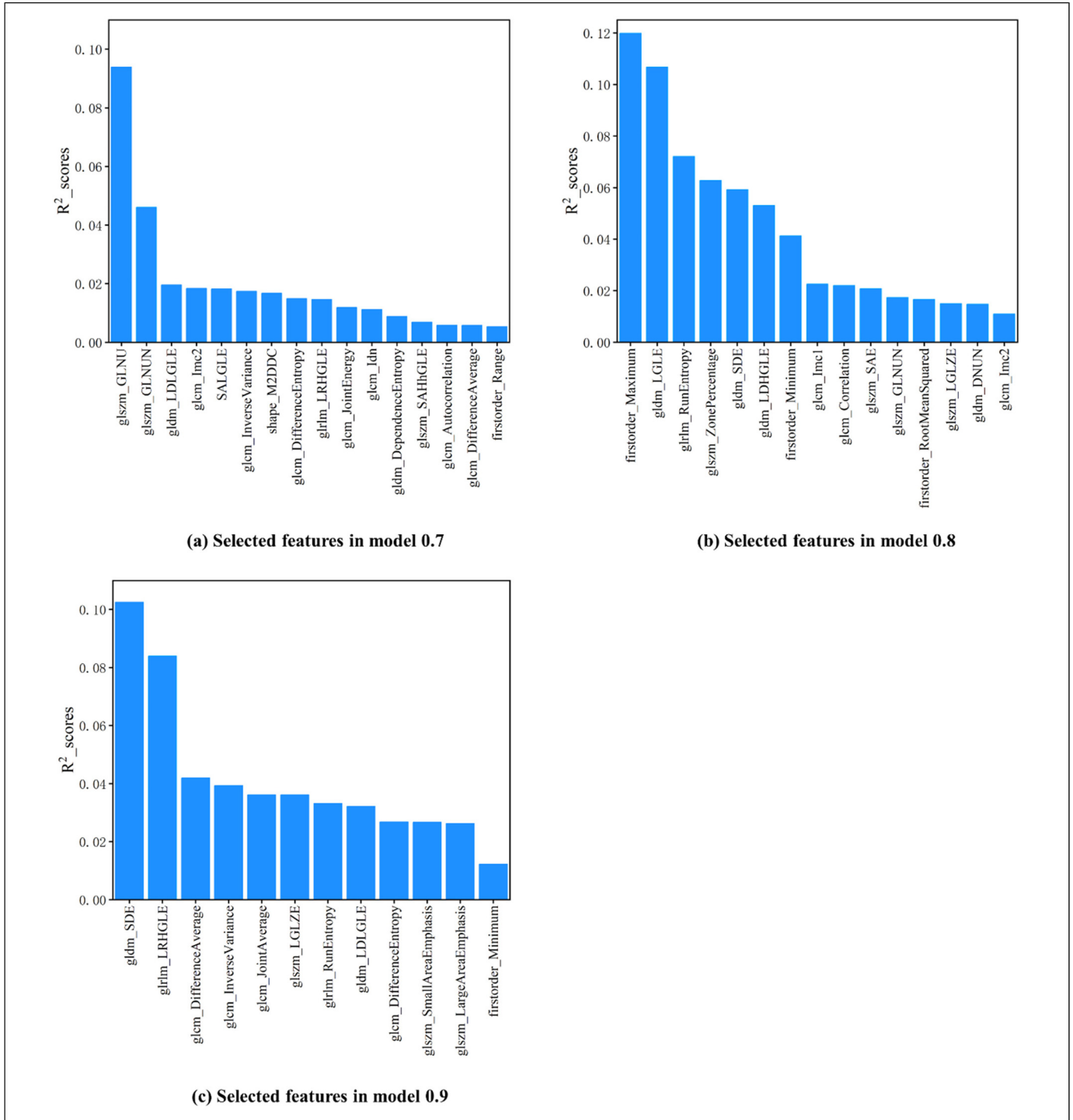


**Figure 3.** Feature importance ranks in the 0.7, 0.8, and 0.9 models obtained by LightGBM-RFECV are shown in (a–c). The  $R^2$  scores were averaged over 5 rounds of independent tests.

predictive ability. The LightGBM-based RFECV method that we used in this work helped reduce data redundancy by lowering the dimensions of features.<sup>48</sup> Hence, the method increased the ratio between the input data dimensions and the filtered feature dimensions, further reducing overfitting.<sup>35</sup> We used a test set for the evaluation of the supervised feature engineering process to avoid

overestimated classification predictive results. The feature importance ranking was consistent during the cross-validation.

There is no relevant research to refer to as the gold standard for the demarcation of the correlation between the external motion and the internal tumor motion. We had to establish 3 models with different classification thresholds (0.7, 0.8, and



**Figure 4.** Summary plots of Kernel Shapley additive explanations (SHAP) in the 3 models. The influence of each selected feature on a prediction is shown as colored plots. The blue and red plots represent lower and higher values of the features, respectively.

0.9) for classification forecasting. To reduce the probability of misjudging low-correlation patients as high-correlation and improve the sensitivity of the model in low-correlation samples, we marked low-correlation samples as positive samples. The ratio of positive to negative samples was approximately 1:4 when the threshold was set to 0.7. To improve the performance, we adopted undersampling and oversampling methods to optimize sample distribution. As the classification threshold increases, more samples are marked as positive samples, which ameliorates the sample distribution. From this process, the sensitivity is improved, and the specificity is slightly reduced. For a comprehensive consideration of sensitivity and specificity, the optimal classification threshold should be set to 0.8.

**Table 2.** Prediction Performance of Different Radiomic Models.

Models	AUC	Sen	Spe	ACC	F-score
0.7	0.837	0.800 ± 0.126	0.771 ± 0.114	0.779	0.656
0.8	0.946	0.829 ± 0.140	0.936 ± 0.058	0.895	0.848
0.9	0.887	0.864 ± 0.086	0.839 ± 0.101	0.853	0.877

Abbreviations: AUC, area under the receiver operating characteristic curve; Sens, sensitivity; Spec, specificity; PPV, positive predictive value; NPV, negative predictive value; ACC, accuracy; the values are reported by the mean in the bracket.

The external/internal correlation cannot simply be derived from patient respiratory and tumor characteristics. The existing exploratory research of the correlation mainly focuses on the measurements of the movement of the whole thoracoabdominal surface<sup>49-51</sup> and improving the accuracy of the correlation through various algorithms. Yu<sup>15</sup> established a 3D voxel model obtaining rich respiratory features of thoracoabdominal torsos, which enhanced the accuracy of tumor motion correlations. Liu et al developed a support vector classification for predicting liver tumor tracking errors based on the features extracted from delivery system log files and achieved good accuracy (AUC = 0.87) at a 2 mm threshold.<sup>52</sup> Okawa et al predicted thoracoabdominal tumor tracking errors within 2.1 mm according to a patient's respiratory waveform.<sup>53</sup> In this study, we developed a model based on tumor radiomic features to achieve similar accurate predictions of external/internal correlation at thresholds of 0.8 and 0.9. Obtaining this information assists in making more appropriate tumor motion tracking strategy decisions and increases treatment profits. Furthermore, as an exploratory study, the overall framework can allow the combination of more advanced correlation measurement methods and other information data, such as body surface movement characteristics. In addition, we included all patients who satisfied the inclusion criteria, and the sample size was sufficient for model training. The inclusion of more samples may result

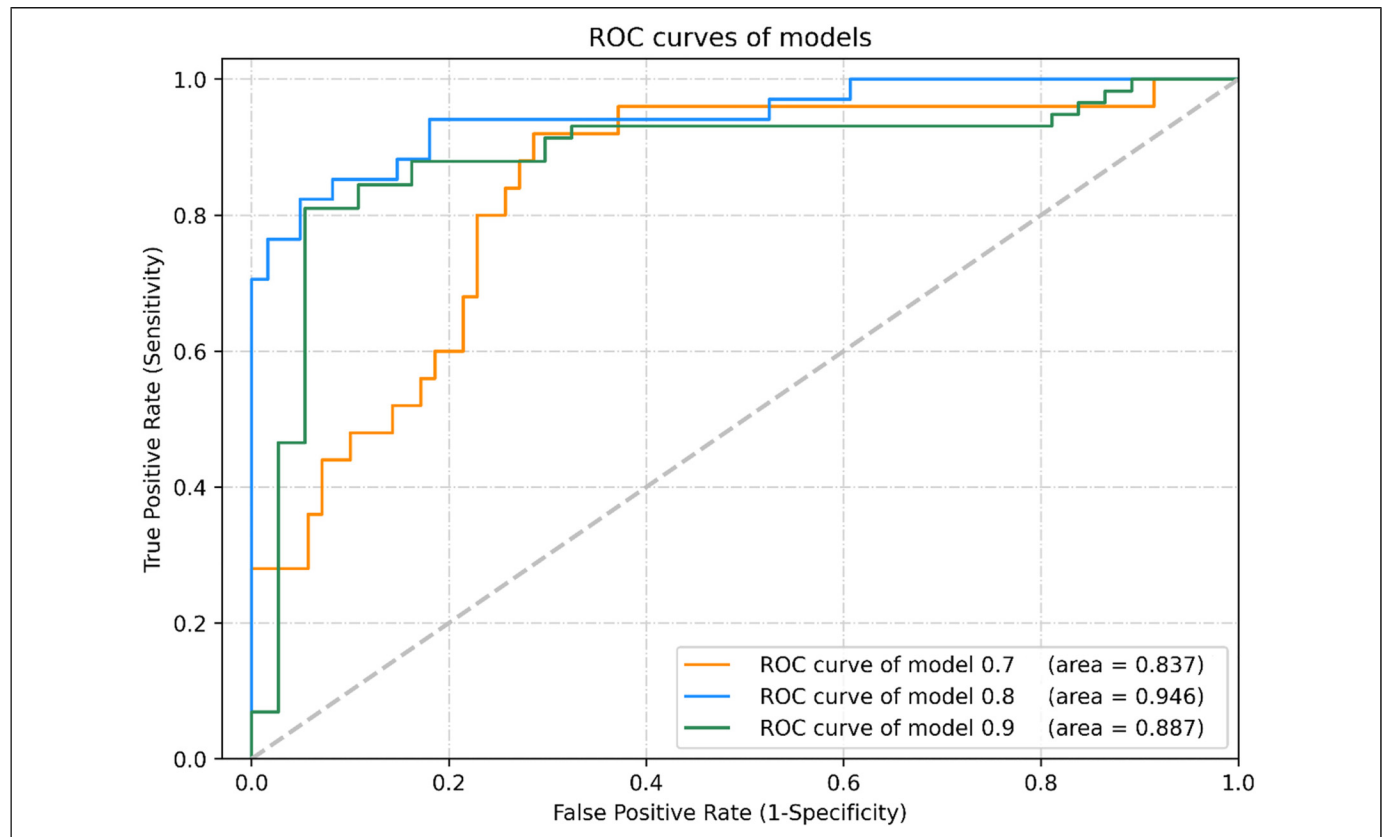


**Figure 5.** ROC curves of the 3 machine learning models. The area under this curve is a measure of the overall predictive utility of the model. The dashed line matching to an AUC of 0.5 indicates performance equal to random guessing.



in performance improvements, which need to be further verified. For a patient whose external/internal correlation is predicted to be high, we recommend using external surrogate position monitoring for indirect tumor tracking. It can reduce both the intrafraction setup uncertainty and prospectively predict the upcoming position of the tumor during treatment, which in return will ensure an adequate dose to the target and a reduced dose to OAR.<sup>54,55</sup> For patients with unsatisfactory correlation, we recommend using other tumor motion tracking methods according to current clinical technology, such as fiducial marker,<sup>56</sup> fluoroscopy imaging,<sup>57</sup> and AI-based motion prediction.<sup>58</sup>

There are several limitations of our study. First, our study has a small sample size, with only 67 patients enrolled. Abundant imaging features extracted in radiomics increase the risk of overfitting, and the inclusion of more samples may result in performance improvements, which need to be further verified.<sup>59</sup> Second, there is no consensus of standardized implementations of the radiomic workflow; wide variation in clinical imaging acquisition parameters can affect image noise and texture and consequently the radiomic features' value.<sup>60</sup> Furthermore, indirect tumor tracking methods require a constant internal/external correlation in clinical practice.<sup>61</sup> There are variations among motion amplitudes and among tumor positions from day to day,<sup>62</sup> and the impact of such variations on the stability of the external/ internal correlation will limit the accuracy of our model and thus requires further study. The stability of the correlation can be guaranteed by acquiring robust motion data. The external/ internal correlation calculated from the body surface motion data (obtained by the audiovisual biofeedback technology) has no statistical difference between before and during treatment, which can be used to ensure the stability of the external/ internal correlation.<sup>63</sup> In addition, appropriate breathing training and voice guidance for patients during the simulated 4DCT period and fractionated treatments can also improve the CCIE stability.<sup>64</sup> In future work, we will further explore the stability of the external/internal correlation. We will look for features that may reflect changes in the external/internal correlation and build a model with predictive stability over interfractions.

## Conclusion

In this study, we determined that the external and internal lung tumor respiratory motion correlation can be reflected by CT radiomic features. We provided a machine learning framework to achieve accurately classified predictions of the correlation, which can assist in determining the motion management strategy for lung tumor patients.

## Acknowledgments

Not applicable.

## Author Contribution

Xiangyu Zhang and Xinyu Song contributed equally to this work.

## Declaration of Conflicting Interests

The author(s) declared no potential conflicts of interest with respect to the research, authorship, and/or publication of this article.




## Ethical Approval

This study was approved by the ethics committee of the West China Hospital with no need for patient consent (No. 2021-86) and registered by the Chinese Clinical trial Registration Center with registration number "ChiCTR2100042714."

## Funding

The author(s) disclosed receipt of the following financial support for the research, authorship, and/or publication of this article: This work was supported by the National Natural Science Foundation of China (grant numbers 81972848, 81472807, and 81803056), and the Sichuan Science and Technology Program (grant number 2021YFS0143).

## ORCID iD

Guangjun Li MS  <https://orcid.org/0000-0003-2054-1771>  
Jing Li PhD  <https://orcid.org/0000-0001-5957-981X>  
Sen Bai  <https://orcid.org/0000-0002-7146-6970>

## Supplemental Material

Supplemental material for this article is available online.

## References

1. Knybel L, Cvek J, Molenda L, et al. Analysis of lung tumor motion in a large sample: patterns and factors influencing precise delineation of internal target volume. *Int J Radiat Oncol Biol Phys*. 2016;96(4):751-758.
2. Dhont J, Vandemeulebroucke J, Burghelea M, et al. The long- and short-term variability of breathing induced tumor motion in lung and liver over the course of a radiotherapy treatment. *Radiother Oncol*. 2018;126(2):339-346.
3. Rusthoven KE, Pugh TJ. Stereotactic body radiation therapy for inoperable lung cancer. *JAMA*. 2010;303(23):2354-2355. author reply 2355.
4. Zhao B, Yang Y, Li T, et al. Dosimetric effect of intrafraction tumor motion in phase gated lung stereotactic body radiotherapy. *Med Phys*. 2012;39(11):6629-6637.
5. Modiri A, Gu X, Hagan A, et al. Inverse 4D conformal planning for lung SBRT using particle swarm optimization. *Phys Med Biol*. 2016;61(16):6181-6202.
6. Yan H, Zhu G, Yang J, et al. The investigation on the location effect of external markers in respiratory-gated radiotherapy. *J Appl Clin Med Phys*. 2008;9(2):57-68.
7. Mueller M, Poulsen P, Hansen R, et al. The markerless lung target tracking AAPM grand challenge (MATCH) results. *Med Phys*. 2022;49(2):1161-1180.
8. Nelson C, Starkschall G, Balter P, et al. Assessment of lung tumor motion and setup uncertainties using implanted fiducials. *Int J Radiat Oncol Biol Phys*. 2007;67(3):915-923.
9. Esmaili Torshabi A, Riboldi M, Imani Fooladi AA, et al. An adaptive fuzzy prediction model for real time tumor tracking in

- radiotherapy via external surrogates. *J Appl Clin Med Phys*. 2013;14(1):4008.
10. Park S, Farah R, Shea SM, et al. Simultaneous tumor and surrogate motion tracking with dynamic MRI for radiation therapy planning. *Phys Med Biol*. 2018;63(2):25015.
  11. Nankali S, Torshabi AE, Miandoab PS. A feasibility study on ribs as anatomical landmarks for motion tracking of lung and liver tumors at external beam radiotherapy. *Technol Cancer Res Treat*. 2017;16(1):99-111.
  12. Dhont J, Harden SV, Chee LYS, et al. Image-guided radiotherapy to manage respiratory motion: lung and liver. *Clin Oncol (R Coll Radiol)*. 2020;32(12):792-804.
  13. Kanoulas E, Aslam JA, Sharp GC, et al. Derivation of the tumor position from external respiratory surrogates with periodical updating of the internal/external correlation. *Phys Med Biol*. 2007;52(17):5443-5456.
  14. Imura M, Yamazaki K, Shirato H, et al. Insertion and fixation of fiducial markers for setup and tracking of lung tumors in radiotherapy. *Int J Radiat Oncol Biol Phys*. 2005;63(5):1442-1447.
  15. Yu S, Hou P, Sun R, et al. Correlated skin surface and tumor motion modeling for treatment planning in robotic radiosurgery. *Front Neurobot*. 2020;14:582385.
  16. Torshabi AE, Pella A, Riboldi M, et al. Targeting accuracy in real-time tumor tracking via external surrogates: a comparative study. *Technol Cancer Res Treat*. 2010;9(6):551-562.
  17. Wang G, Li Z, Li G, et al. Real-time liver tracking algorithm based on LSTM and SVR networks for use in surface-guided radiation therapy. *Radiat Oncol*. 2021;16(1):13.
  18. Ernst F, Bruder R, Schlaefler A, et al. Correlation between external and internal respiratory motion: A validation study. *Int J CARS*. 2012;7(3):483-492.
  19. Wijenayake U, Park S-Y. Real-time external respiratory motion measuring technique using an RGB-D camera and principal component analysis. *Sensors (Basel)*. 2017;17(8):1840.
  20. Keall PJ, Mageras GS, Balter JM, et al. The management of respiratory motion in radiation oncology report of AAPM task group 76. *Med Phys*. 2006;33(10):3874-3900.
  21. Seppenwoolde Y, Shirato H, Kitamura K, et al. Precise and real-time measurement of 3D tumor motion in lung due to breathing and heartbeat, measured during radiotherapy. *Int J Radiat Oncol Biol Phys*. 2002;53(4):822-834.
  22. Wang G, Song X, Li G, et al. Correlation of optical surface respiratory motion signal and internal lung and liver tumor motion: a retrospective single-center observational study. *Technol Cancer Res Treat*. 2022;21:15330338221112280.
  23. Tsunashima Y, Sakae T, Shioyama Y, et al. Correlation between the respiratory waveform measured using a respiratory sensor and 3D tumor motion in gated radiotherapy. *Int J Radiat Oncol Biol Phys*. 2004;60(3):951-958.
  24. Liu HH, Koch N, Starkschall G, et al. Evaluation of internal lung motion for respiratory-gated radiotherapy using MRI: part II-margin reduction of internal target volume. *Int J Radiat Oncol Biol Phys*. 2004;60(5):1473-1483.
  25. Hoisak JD, Sixel KE, Tirona R, et al. Correlation of lung tumor motion with external surrogate indicators of respiration. *Int J Radiat Oncol Biol Phys*. 2004;60(4):1298-1306.
  26. Du Q, Baine M, Bavitz K, et al. Radiomic feature stability across 4D respiratory phases and its impact on lung tumor prognosis prediction. *PLoS One*. 2019;14(5):e0216480.
  27. Kumar V, Gu Y, Basu S, et al. Radiomics: the process and the challenges. *Magn Reson Imaging*. 2012;30(9):1234-1248.
  28. Lambin P, Rios-Velazquez E, Leijenaar R, et al. Radiomics: extracting more information from medical images using advanced feature analysis. *Eur J Cancer*. 2012;48(4):441-446.
  29. Hu J, Zhao Y, Li M, et al. Machine learning-based radiomics analysis in predicting the meningioma grade using multiparametric MRI. *Eur J Radiol*. 2020;131:109251.
  30. Hosny A, Parmar C, Coroller TP, et al. Deep learning for lung cancer prognostication: a retrospective multi-cohort radiomics study. *PLoS Med*. 2018;15(11):e1002711.
  31. Oikonomou A, Khalvati F, Tyrrell PN, et al. Radiomics analysis at PET/CT contributes to prognosis of recurrence and survival in lung cancer treated with stereotactic body radiotherapy. *Sci Rep*. 2018;8(1):4003.
  32. Lafata K, Cai J, Wang C, et al. Spatial-temporal variability of radiomic features and its effect on the classification of lung cancer histology. *Phys Med Biol*. 2018;63(22):225003.
  33. Hosseini SA, Shiri I, Hajianfar G, et al. Synergistic impact of motion and acquisition/reconstruction parameters on 18 F-FDG PET radiomic features in non-small cell lung cancer: phantom and clinical studies. *Med Phys*. 2022;49(6):3783-3796.
  34. Adachi T, Nagasawa R, Nakamura M, et al. Vulnerabilities of radiomic features to respiratory motion on four-dimensional computed tomography-based average intensity projection images: a phantom study. *J Appl Clin Med Phys*. 2022;23(3):e13498.
  35. Collins GS, Reitsma JB, Altman DG, et al. Transparent reporting of a multivariable prediction model for individual prognosis or diagnosis (TRIPOD): the TRIPOD statement. *BMC Med*. 2015;67(6):1142-1151.
  36. Guckenberger M, Andratschke N, Dieckmann K, et al. ESTRO ACROP consensus guideline on implementation and practice of stereotactic body radiotherapy for peripherally located early stage non-small cell lung cancer. *Radiother Oncol*. 2017;124(1):11-17.
  37. Griffiths D. A pragmatic approach to spearman's rank correlation coefficient. *Teach Stat*. 1980;2(1):10-13.
  38. Korin HW, Ehman RL, Riederer SJ, et al. Respiratory kinematics of the upper abdominal organs: a quantitative study. *Magn Reson Med*. 1992;23(1):172-178.
  39. Zwanenburg A, Vallières M, Abdalah MA, et al. The image biomarker standardization initiative: standardized quantitative radiomics for high-throughput image-based phenotyping. *Radiology*. 2020;295(2):328-338.
  40. Scott M. Lundberg and Su-In Lee. A Unified Approach to Interpreting Model Predictions.
  41. Bai HX, Lee AM, Yang L, et al. Imaging genomics in cancer research: limitations and promises. *Br J Radiol*. 2016;89(1061):20151030.
  42. Chawla NV, Bowyer KW, Hall LO, et al. SMOTE: synthetic minority over-sampling technique. *JAIR*. 2002;16:321-357.
  43. Hosmer DW, Lemeshow S. *Applied Logistic Regression*. 2nd ed. Wiley; 2000.

44. Wei L, Osman S, Hatt M, et al. Machine learning for radiomics-based multimodality and multiparametric modeling. *Q J Nucl Med Mol Imaging*. 2019;63(4):323-338.
45. Mayerhoefer ME, Szomolanyi P, Jirak D, et al. Effects of MRI acquisition parameter variations and protocol heterogeneity on the results of texture analysis and pattern discrimination: an application-oriented study. *Med Phys*. 2009;36(4):1236-1243.
46. Larue R, van de Voorde L, van Timmeren JE, et al. 4DCT Imaging to assess radiomics feature stability: an investigation for thoracic cancers. *Radiother Oncol*. 2017;125(1):147-153.
47. Avanzo M, Wei L, Stancanella J, et al. Machine and deep learning methods for radiomics. *Med Phys*. 2020;47(5):e185-e202.
48. Zhou D, Zhuang X, Zuo H, et al. Deep learning-based approach for civil aircraft hazard identification and prediction. *IEEE Access*. 2020;8:103665-103683.
49. Gu C, Li C. Assessment of human respiration patterns via noncontact sensing using Doppler multi-radar system. *Sensors (Basel)* 2015;15(3):6383-6398.
50. Transue S, Nguyen P, Vu T, et al. Real-time tidal volume estimation using iso-surface reconstruction. In: 2016 IEEE First International Conference on Connected Health: Applications, Systems and Engineering Technologies (CHASE), Washington, DC, USA, 2016/6/27–2016/6/29. IEEE, pp.209-218.
51. Ernst F, Saß P. Respiratory motion tracking using Microsoft's Kinect v2 camera. *Curr Dir Biomed Eng*. 2015;1(1):192-195.
52. Liu M, Cygler JE, Vandervoort E. Patient-specific PTV margins for liver stereotactic body radiation therapy determined using support vector classification with an early warning system for margin adaptation. *Med Phys*. 2020;47(10):5172-5182.
53. Okawa K, Inoue M, Sakae T. Development of a tracking error prediction system for the CyberKnife synchrony respiratory tracking system with use of support vector regression. *Med Biol Eng Comput*. 2021;59(11-12):2409-2418.
54. Hoisak JDP, Pawlicki T. The role of optical surface imaging systems in radiation therapy. *Semin Radiat Oncol*. 2018;28(3):185-193.
55. Freislederer P, Kügele M, Öllers M, et al. Recent advanced in surface guided radiation therapy. *Radiat Oncol*. 2020;15(1):187.
56. Shirato H, Harada T, Harabayashi T, et al. Feasibility of insertion/implantation of 2.0-mm-diameter gold internal fiducial markers for precise setup and real-time tumor tracking in radiotherapy. *Int J Radiat Oncol Biol Phys*. 2003;56(1):240-247.
57. Tang X, Sharp GC, Jiang SB. Fluoroscopic tracking of multiple implanted fiducial markers using multiple object tracking. *Phys Med Biol*. 2007;52(14):4081-4098.
58. Rostampour N, Jabbari K, Esmaili M, et al. Markerless respiratory tumor motion prediction using an adaptive neuro-fuzzy approach. *J Med Signals Sens*. 2018;8(1):25.
59. Avanzo M, Stancanella J, El Naqa I. Beyond imaging: the promise of radiomics. *Phys Med*. 2017;38:122-139.
60. Rizzo S, Botta F, Raimondi S, et al. Radiomics: the facts and the challenges of image analysis. *Eur Radiol Exp*. 2018;2(1):36.
61. Berbeco RI, Nishioka S, Shirato H, et al. Residual motion of lung tumours in gated radiotherapy with external respiratory surrogates. *Phys Med Biol*. 2005;50(16):3655-3667.
62. Ge J, Santanam L, Noel C, et al. Planning 4-dimensional computed tomography (4DCT) cannot adequately represent daily intrafractional motion of abdominal tumors. *Int J Radiat Oncol Biol Phys*. 2013;85(4):999-1005.
63. Lee D, Greer PB, Paganelli C, et al. Audiovisual biofeedback improves the correlation between internal/external surrogate motion and lung tumor motion. *Med Phys*. 2018;45(3):1009-1017.
64. Huguet F, Yorke ED, Davidson M, et al. Modeling pancreatic tumor motion using 4-dimensional computed tomography and surrogate markers. *Int J Radiat Oncol Biol Phys*. 2015;91(3):579-587.